Aircraft Characterization in Icing Using Flight Test Data

Edward A. Whalen,[#] James W. Melody,[♦] Michael B. Bragg[+] and Tamer Başar[*]
University of Illinois at Urbana-Champaign, Urbana, IL 61801

ABSTRACT

The University of Illinois, in conjunction with NASA Glenn, has conducted a flight test program to investigate aircraft icing effects and develop aircraft icing effects characterization techniques. Flights were conducted in 2001 and 2002 to collect data in clear air as well as in natural icing conditions. These data were used to identify the effects of icing on aircraft performance and control. It was also used to aid in the development of an H^{∞} characterization algorithm being designed specifically for the Smart Icing System (SIS).

Flight test data analysis was accomplished using a modified stepwise regression technique. Systems IDentification Programs for Aircraft (SIDPAC) was used for the linear regression analysis. The results of this analysis revealed multiple parameters that clearly indicated both the presence and severity of the ice accretion. Atmospheric turbulence was shown to significantly affect this method of parameter identification.

A real-time H^{∞} parameter identification (PID) algorithm has previously been developed as part of the icing characterization function of the Smart Icing System. This paper presents an initial validation of the H^{∞} PID algorithm wherein the algorithm is applied to the flight test data after the fact, but in a manner that is consistent with the ultimate real-time application. This mock real-time validation demonstrates that the H^{∞} PID algorithm provides pitching moment derivative estimates that are consistent with those provided by SIDPAC for both clear-air and icing conditions in the absence of turbulence. As with the stepwise regression technique, the H^{∞} PID algorithm has degraded accuracy in atmospheric turbulence.

INTRODUCTION

The effect of ice accretion on aircraft has been observed and investigated since the mid 1900's. Aircraft icing degrades both the performance and control of aircraft by disrupting the flow of air over the aircraft. Excessive accretion can lead to flow separation and stall of both the main wing and tail. Incidents such as the American Eagle roll upset near Roselawn, Indiana in October 1994 and the Com Air accident in January 1997 are just two examples of the dangers of aircraft icing. Quantifying the amount of ice accretion and its effect on the aircraft and when the aircraft has reached the edge of its flight envelope is a difficult proposition. Different icing conditions lead to different types, sizes and locations of ice accretion, which may or may not lead to significant loss of control and performance. The most straightforward way to monitor the effect of any type of icing is to measure, in flight, the stability and control derivatives and the trim state for the aircraft. Any changes in these values, outside of those changes expected for a clean aircraft, would indicate that something, in this case icing, is affecting the control and performance of the aircraft.

Research into the effects of icing on aircraft has been ongoing since the mid-1940's when investigations into the effect of icing on propellers became a concern.[1] More recently, an investigation by Ranaudo, et al.[2] found that glaze icing led to a decrease in lift of up to 10% and increased drag up to 55%. Estimates of stability and control derivatives for the Twin Otter were calculated from flight data, using a maximum likelihood method, by Ranaudo, et al. in 1986.[3] Reductions of 10 to 15% in pitching moment, elevator power and elevator effectiveness were documented. Ratvasky and Ranaudo[4] observed similar results in 1993 using a modified stepwise regression analysis. They also recorded reductions in static stability of up to

[#] Graduate Research Assistant, Department of Aerospace Engineering.
[♦] Graduate Research Assistant, Dept. of Elec. and Comp. Eng. and the Coordinated Sciences Laboratory.
[+] Professor and Head, Department of Aerospace Engineering, Fellow AIAA.
* Professor, Dept. of Elec. And Comp. Eng. and the Coordinated Sciences Laboratory.

10% and reductions in directional stability of up to 20% for the zero thrust case. A recent NASA tailplane icing study[5] revealed significant reductions, over 30%, in elevator effectiveness with 40° flap deflection as well as strong static instability at high angles of attack with 20 and 30 degrees of flap deflection. These results were indicative of the problems leading to icing incidents during approach to landing.

An interdisciplinary team of researchers from the University of Illinois at Urbana-Champaign, the Ohio State University and NASA Glenn has conducted the fundamental research necessary to develop a smart icing system (SIS) to improve the safety of operations in icing conditions. This research used a systems approach examining the aircraft operational system including flight mechanics, aircraft control and human factors. Bragg et al.[6] in 2002 provided an overview of the research program and its motivation.

The control center of the envisioned smart icing system was the ice management system (IMS) that performed the functions below.[7,8]

1. Sense the effect of ice accretion on aircraft performance, stability and control. Sense ice accretion and ice protection system performance. Provide the appropriate information to the flight crew.
2. Automatically activate and manage the ice protection systems, and provide the pilot with feedback on the system status and behavior of both the aircraft and the ice protection system.
3. Modify the aircraft flight envelope by use of the flight control system to avoid conditions where flight could potentially be uncontrollable. Notify the flight crew of this action and its implications for the flight envelope.
4. Adapt the aircraft control laws to maintain clean-aircraft-like flying qualities to enable the aircraft to be safely flown within the reduced flight envelope. Notify the flight crew of this action and maintain good pilot-automation coordination.

In the winter of 2001 and 2002 a flight test program was conducted, with the support of NASA Glenn, to aid in the development of the SIS. The primary goal was to identify the parameters that best indicated the onset of icing and the effects of various levels of icing on the performance and control of the aircraft. Additionally, it was important to identify the activation of the deicing system of the aircraft. To accomplish this, stability and control derivatives were extracted from the flight data using SIDPAC in addition to trim and atmospheric data.

The second goal of the flight test program was to help develop and potentially validate the real-time H^{∞} parameter identification (PID) algorithm on flight test data. The algorithm was applied to raw flight test data after the flight tests, but in a manner that is consistent with a real-time implementation, namely, by allowing the PID algorithm at any time instant to have access only to the measurements up to that time instant. The PID algorithm provided estimates of lift, drag, and pitching moment stability and control derivatives at each sample instant by operating on short windows of flight test data that contained elevator doublets. The final value of these estimates is then compared to the SIDPAC estimates for the same data window. Both clear-air and natural-icing flight test cases were used in the validation.

This paper reports on the flight test program and presents SIDPAC and H^{∞} results for the iced flight test. Initial results presented by Whalen, et al.[9] provided details of the flight test program and initial SIDPAC results. Here, results are expanded to investigate the use of trim data to identify the performance effects and H^{∞} results are presented for the first time.

FLIGHT TEST METHODS AND PROCEDURES

NASA Twin Otter Research Aircraft

NASA's Icing Research Aircraft used in the flight test is a modified DeHavilland DHC-6 Twin Otter. It is a high-wing, twin-engine, commuter class aircraft that has been outfitted with additional ice protection equipment and instrumentation to measure icing meteorological conditions, document resultant ice accretions, and measure aircraft performance degradation. The Icing Research Aircraft's maximum gross weight is 11,000 pounds, cruises at approximately 130 KIAS and has an operating range of approximately 300 nautical miles. Further details concerning the Twin Otter can be found in Whalen, et.al..

The icing research data system flown on the Twin Otter incorporated the following components: 1) cloud physics instruments, 2) air data instruments, 3) global positioning system, and 4) signal conditioning, data acquisition, display and recording systems. Each of these components will be described below.

Ice accretion documentation was accomplished with 1) a wing stereo photography system, 2) continuous video taping of the right wing leading edge, and 3) a hand-held 35 mm camera. The wing stereo photography system consisted of two 70 mm format Hasselblad cameras with 250 mm lenses mounted in the nose of the aircraft behind optical glass view ports. The objective of this system was to obtain stereo pair photo images of the wing's leading edge that would enable measurements of the ice surface through photogrammetric analysis to generate profiles (two-dimensional slices) of the ice shape with a minimum acceptable resolution of ±0.03 inch.

Aircraft performance degradation was determined using the previously described air data instrumentation, an inertial package, and engine/prop data. Inertial sensors consisted of three orthogonally mounted linear accelerometers, three orthogonally mounted angular rate gyros, and a vertical gyro to provide pitch and roll angle data. These sensors were mounted near the aircraft center of gravity. Thrust calculations were made by measuring propeller RPM and engine torque values to determine propeller advance ratio and engine power coefficient. Thrust coefficient was then determined using Hartzell propeller data tables. These sensors enabled real-time calculation of overall aircraft lift and drag performance.

Test Matrix

Table 1 is a condensed summary of the test matrix of the flight test program. As stated earlier, the test matrix was categorized into two major components: clear-air flights and iced flights. In 2001, a total of 9 flights were conducted, four of which were in icing conditions. Much of the flight time in 2001 was spent establishing a clean baseline aircraft and collecting data across the entire test matrix. In addition to establishing a good clean aircraft model, identification maneuvers and key icing parameters were established. The 2002 test focused on identifying icing severity, icing onset and deicing. Of the 15 flights completed, 11 were in icing conditions. Emphasis was placed on cases 2.1 through 2.3.

SYSTEM CHARACTERIZATION METHODS

A desirable way to monitor the effect of any type of icing on an aircraft is to measure the stability and control derivatives as well as the trim state. Using a set of programs called System Identification Programs for AirCraft[10] (SIDPAC), stability and control derivatives were extracted from the dynamic response of the aircraft to input control doublets. E. A. Morelli, at NASA Langley Research Center, developed SIDPAC. SIDPAC provided linear, quasi-steady state identification from flight data. Results from this analysis are presented in this paper including: icing effects, detection of IPS activation and correlations with icing severity.

Another identification method is currently being developed at the University of Illinois. This Parameter IDentification (PID) algorithm seeks to characterize the effects of icing on the aircraft flight dynamics by observing its input (elevator, aileron, rudder angles as well as power) and its output (angular rates, angle of attack, sideslip angle, total velocity, etc.) and inferring from these observations a real-time estimate of a "parameter" that describes the flight dynamics behavior, namely a vector of stability and control derivatives. The PID algorithm has recently been modified to incorporate translational acceleration measurements. Utilizing these measurements in the algorithm was the key to providing useful lift derivative estimates. Previously, several PID algorithms have been evaluated in extensive simulation studies,[11,12] and a recursive H^{∞} PID algorithm has been chosen for its robustness to unmeasured disturbance input (such as turbulence) and sensor noise. The H^{∞} PID algorithm seeks to achieve a guaranteed disturbance attenuation ratio between the unknown exogenous signals, i.e., disturbance and sensor noise, by assuming worst-case values for the deleterious signals, and is described by a set of coupled ordinary differential equations.[6] In order to be implemented in real time on a digital computer, the ODEs are converted to discrete-time difference equations using the standard fourth-order Runge-Kutta technique.

RESULTS AND DISCUSSION

SIDPAC Results

Whalen, et al., in 2002, presented preliminary results from these flight tests. The analysis presented here includes improvements in the analysis technique, the addition of the trim state analysis, investigations of selective deicing and the addition of the icing severity parameter, η. Results were improved over the previous analysis by using corrected values for the aircraft moments of inertia and center of gravity, including more steady state data before each doublet and dynamic data following each doublet. Nose boom oscillations, at 7 Hz, were discovered following the 2001 flight test. The oscillations in these data were filtered in post-processing, however during the 2002 tests the oscillations were filtered in-flight. In both cases a 10 Hz, low pass filter was used to remove the oscillations.

In order to evaluate the effect of icing on aircraft control and performance an entire flight through icing conditions is presented. Flight 010302f1 is used because it contains clean control doublets as well as control doublets in icing and after selective deicing. Atmospheric conditions for the flight are presented in Figs. 1–3. Figure 1 presents the LWC, Fig. 2 presents the temperature and Fig. 3 presents the MVD during the flight. The magnitude of the ice accretion, as described by the icing severity parameter, η[13], is presented in Fig. 4. Figures 5 and 6 present the variation in $C_{L\alpha}$ and $C_{M\alpha}$, respectively, during the icing encounter. The change in parasite drag, with respect to the clean aircraft, is also presented as Fig. 7. Degradations in both stability parameters and the parasite drag are visible due to ice accretion. Additionally, the activation of the IPS system, using selective deicing is apparent in the data. Residual ice is also clearly indicated in the parasite drag data.

On the day of flight 010302f1, the weather briefing predicted good glaze icing conditions throughout the flight test area. The LWC was approximately 0.3 g/m^3 for the majority of the flight, but fell to 0.1 to 0.2 g/m^3 towards the end of the flight (Fig. 1). This, coupled with a static temperature of approximately -5° C, (Fig. 2) resulted in glaze icing. As presented in Fig. 3, the MVD remained at approximately 18 μm for the majority of the flight. Figure 4 presents the variation of η, which was referenced to the main wing of the airplane. Three distinct icing encounters are visible in the plot of η. Perfect deicing was assumed in that figure, that is, when the deicing system was activated η was reset to zero.

Figure 5 is an annotated plot of $C_{L\alpha}$. The annotation was included to aid in the understanding of what was occurring during the flight with respect to icing and IPS operation. Each marked data point on the plot is a doublet set, which consisted of two elevator doublets, an aileron doublet and a rudder doublet. The lines connecting the doublets are illustrative only and are not the result of data. The value of R^2 for the lift derivative estimates was greater than 90% for all the maneuvers. The trim lift coefficient remained between 0.5 and 0.7 over the entire flight.

Initially, the LWC was zero while the Twin Otter completed a baseline doublet set before entering icing conditions. The value of $C_{L\alpha}$ for that doublet was 0.0925 deg^{-1}. The low value of the clean estimation was attributed to the fact that the atmospheric conditions may have allowed some ice to accrete on the aircraft. Furthermore, the values of the biases and scaling factors for that maneuver were consistent with some effect due to turbulence. Following that the aircraft was allowed to accrete ice for about 20 minutes and then another doublet was carried out. During the encounter the LWC and MVD were steady at 0.35 g/m^3 and 18 μm, respectively. The value of $C_{L\alpha}$ dropped approximately 13%, to 0.0818 deg^{-1}. Also, the value of $C_{M\alpha}$ increased (i.e. became more positive) by approximately 4% over the value of the first doublet and almost 20% over the baseline value (Fig. 6). The parasite drag coefficient (referenced to the clean aircraft), shown in Fig. 7, increased by 0.0233 during the icing encounter.

The aircraft was then flown out of the icing cloud and stereo photography pictures were taken. Figure 8 is a photograph of the right wing leading edge at 14:04:31. The stereo photograph profile (Fig. 9) revealed that the maximum ice thickness midway between the wing fences on the top surface was 0.33" and the maximum thickness on the lower surface was 0.41". A doublet was carried out shortly after that at 14:06. The high value of $C_{L\alpha}$ that was estimated did not agree well with other indicators of icing. Although ice could have been shed from the aircraft during the time between the first and third doublet, the parasite drag indicated no such loss of ice. At the time of the following deicing 5/8" of ice accretion was reported in the flight log. The inconsistent estimation was most likely not due to turbulence effects since the aircraft was above the clouds and no unusual scaling factors or biases were calculated. The entire aircraft was then deiced at 14:09 and another doublet set was carried out with some residual ice on the unprotected parts of the aircraft. The value of $C_{L\alpha}$ did not change significantly from the previous estimation, indicating that there was still ice on the wing affecting its performance. The parasite drag was consistently 0.02 higher, or greater, than the baseline value, indicating that the aircraft carried ice in unprotected areas throughout the encounter.

At 14:11 the aircraft descended back into the icing cloud to accrete ice for approximately 24 minutes before the next doublet set. LWC fluctuated between 0.1 and 0.4 g/m^3 during that encounter. MVD also fluctuated between 10 and 20 μm. Smaller chordwise accretion was reported as well as ¼" of ice on the struts. Both $C_{L\alpha}$ and $C_{M\alpha}$ showed little change due to this accretion. The parasite drag increased dramatically, to 0.0282 higher than the baseline value.

Figure 10 is a photograph of the right wing leading edge at 14:34:57 during the ice accretion leading up to the selective deicing sequence beginning at 14:38. The ice profile in Fig. 11 shows a top horn approximately 0.45" thick and a lower accretion approximately 0.26" thick. A selective deicing sequence began shortly after the all iced doublet at 14:35. First the wings were deiced, resulting in a recovery of $C_{L\alpha}$ to the baseline clean value. The value of $C_{M\alpha}$ fell to a more negative value than the baseline aircraft because the aircraft was operating at a lift coefficient of 0.6. The greater effectiveness of the elevator was consistent with previous observations made during the clean data analysis. However, the increase was greater than that seen for the clean aircraft and no such effect was seen in $C_{L\alpha}$ as would be expected. Deicing the wings also resulted in a large reduction in parasite drag, from 0.0282 to 0.0216 above the clean value. Next, the horizontal tail was deiced. This resulted in little to no change of the variables presented. Finally, the vertical tail and struts were deiced. The values of the stability derivatives showed little change, but again there was a significant reduction in parasite drag attributed to the removal of the ice.

Following the selective deicing sequence the aircraft descended back into the icing cloud to carry out multiple doublets during ice accretion. During that period the LWC was significantly lower than before, at approximately 0.15 g/m^3, and MVD fluctuated between

10 and 20 μm. The first doublet set was carried out at 14:49 and showed a significant decrease in $C_{L\alpha}$ of approximately 30%, to 0.07544 deg^{-1}, and an increase in $C_{M\alpha}$ of 33% to 0.0205 deg^{-1}. The parasite drag coefficient increased to 0.03 greater than the clean value, indicating that a significant amount of ice had accreted on the aircraft. The flight log verified this by reporting one-quarter inch of ice on the struts during this doublet. Seven minutes later, at 14:56, another set was carried out, this time with 3/8" of ice reported on the struts. Figure 12 is a photograph of the ice accretion on the right wing leading edge at that point. The value of $C_{L\alpha}$ was almost 16% less than the clean baseline value and the value of $C_{M\alpha}$ was almost 7% greater than the clean baseline value. However, the value of $C_{L\alpha}$ increased, indicating that some ice on the wing had naturally shed from the aircraft. Only a slight increase in the parasite drag was seen as a result of the icing. The aircraft then spent fourteen more minutes in icing before the final iced set was completed at 15:10. Again, significant changes in $C_{M\alpha}$ and $C_{L\alpha}$ were observed. $C_{L\alpha}$ decreased almost 25% from the clean value, to 0.087 deg^{-1}. $C_{M\alpha}$ also increased over 20%, to 0.0207 deg^{-1}. The reduction in the parasite drag indicated that some ice had shed from the aircraft during the encounter.

Figure 13 is a photograph of the right wing leading edge at 15:13:05, just prior to deicing. The reduced stereo photograph (Fig. 14) showed that the ice at that time was approximately 0.32" thick on the upper surface of the leading edge and 0.39" thick on the lower surface. The entire aircraft was deiced at 15:14 following a climb above the icing cloud to take photographs. Both $C_{M\alpha}$ and $C_{L\alpha}$ returned to within 10% of the clean values. The parasite drag coefficient decreased to 0.0218 greater than the baseline value. This again showed that the deicing had significantly improved the stability derivatives of the aircraft, but that there was still a significant amount of ice on the aircraft.

A typical selective deicing sequence is depicted in Figs. 15 and 16. Figure 15 presents the value of $C_{L\alpha}$ during the process. A set of doublets were carried out before entering icing and then after each component was deiced. In the sequence the wings were deiced first, followed by the horizontal stabilizer and finally by the vertical stabilizer, wing struts and landing gear. The aircraft was in icing conditions for approximately 20 minutes prior to the selective deicing. Figure 15 shows that, as expected, the only surface that significantly affected the value of $C_{L\alpha}$ was the wing. This was because $C_{L\alpha}$ is directly related to the aerodynamic performance of the wing. The flight log reported "lots of residuals" on the wing following the deicing, which led to a value of $C_{L\alpha}$ 7% below the clean value. Figure 16 reveals the effect, on C_{D0}, of deicing the other components of the aircraft. Deicing the wing at 13:55 and the vertical stabilizer, wing struts and landing gear at 14:02 had the largest impact on the drag coefficient. Deicing the horizontal stabilizer had little to no effect on the drag. This result is intuitive when one considers that the horizontal stabilizer represents the smallest area, by far, deiced in the process.

Figures 17 and 18 present $C_{L\alpha}$ and C_D during an icing encounter with the deicing boots set on an automatic three-minute cycle. Control doublets were carried out immediately following the activation of the deicing boots. Icing conditions, as reported in the flight log, included an LWC of 0.2 g/m^3 and a total temperature of -2.4 °C. The aircraft was in icing conditions for approximately 30 minutes. The boot cycle consistently returned the value of $C_{L\alpha}$ to greater than 0.1 deg^{-1} for the duration of the icing encounter. Data to estimate the value of $C_{L\alpha}$ immediately before deicing was not collected. However, Fig. 18 shows that ice was continually accreting on unprotected areas of the aircraft, resulting in the drag coefficient increasing throughout the encounter. The final parasite drag coefficient was approximately 25% higher than the baseline value.

It was possible to correlate icing effects to the icing severity parameter η. The parasite drag showed a particularly good correlation with η, as shown in Fig. 19. However, none of the stability and control parameters were well correlated with the parameter. Significant errors in the parameter identification were encountered due to atmospheric turbulence. This phenomenon was most likely the cause of the poor correlations with η.

The effects of atmospheric turbulence on the parameter estimations, specifically on $C_{L\alpha}$, are presented in Fig. 20. SIDPAC identification incorporates an instrument calibration step that uses a data compatibility analysis based on the kinematic relations of the flight dynamics to provide maximum likelihood estimates of instrument biases and scale factors. It can be seen that in icing conditions the value of the alpha scale factor varies widely over the maneuvers. Ideally, the scale factor would be zero if the flight data were consistent with the kinematic relations. However, since the kinematic relations used in the data compatibility analysis do not include turbulence effects, the turbulence can result in biased estimates of the instrument scale factors and biases. These biased estimates, in turn, may introduce biases into the S/C derivative estimates. Atmospheric turbulence is typically associated with icing conditions, and was observed in the aircraft z-accelerations during these maneuvers. Therefore, it was concluded that atmospheric turbulence was causing the variations and,

consequently, some erroneous parameter estimates. However, C_{D0} estimations were not affected by the turbulence and are capable of indicating icing onset as well as overall icing severity.

An investigation of the trim state of the airplane further reinforced the utility of parasite drag estimation in the identification of aircraft icing. Figure 21 is a plot of δe versus C_D and Fig. 22 is a plot of δe versus α for various icing encounters. In each figure, data from Flight 010223f2 was included to establish a clean trim curve. Two icing flights are considered here and both were conducted at approximately 130 knots or greater; the clean trim point near zero degrees angle of attack was also obtained at 130 knots. Selective deicing was used during Flight 010302f1, as discussed earlier in this paper, and the stability and control derivatives varied throughout the flight. Figure 21 clearly showed that the drag of the aircraft increased abnormally with respect to the clean airplane. Although the airplane was in steady level flight at or above the airspeed for trim at zero degrees angle of attack in a clean configuration, it was cruising at one to two degrees angle of attack. In addition, Fig. 22 indicated that, at the same time, the elevator deflection required to trim at the same angle of attack increased when compared to the clean curve. Thrust coefficient was slightly higher for flight 010302f1, $C_T \sim 0.08$, versus the baseline, $C_T \sim 0.06$. However, Ratvasky and Ranaudo showed that elevator effectiveness increased with thrust coefficient, which is the opposite of the trend observed. Contrast that with a flight such as 020221f1, wherein the drag was greatly increased while the trim angle of attack remained relatively unchanged. During flight 020221f1 the airplane was deiced component by component once and completely deiced for the final doublet maneuvers. The airplane maintained steady level flight over an angle of attack range of approximately 1 degree, with a significant increase in drag of up to 50% over the baseline value. However, the increase in elevator deflection to trim, when compared to the clean curve, was small and much less pervasive, compared to flight 010302f1. In the first case, the airplane flew at one to two degrees greater angle of attack to maintain steady level flight. At the same time, it required increased elevator deflection to trim. The airplane was experiencing a substantial loss in wing performance coupled with a reduction in elevator effectives. It experienced this even with the operation of the IPS. In the second case, the airplane was able to maintain steady level flight at clean trim angles of attack with little increase in elevator deflection. However, the drag increased dramatically, even with the IPS operating. Both of these cases were conducted at similar flight conditions in glaze icing, but the effects on the airplane were vastly different. Using trim to identify the existence and effects of icing is clearly a valuable tool.

H^∞ Results

The H^∞ PID algorithm was validated by comparing the final values of its S/C derivative estimates with the corresponding SIDPAC estimates. Twenty-six clear-air cases and eight natural icing cases were considered, each of which contained an elevator doublet. Approximately 20 total seconds of data were used for each of the H^∞ estimates.

Although the H^∞ PID algorithm provided estimates for lift, drag, and pitching moment derivatives, only the $C_{L\alpha}$ estimate and pitching moment derivative estimates were found to be useful. This was because the drag derivative estimates as well as the lift derivative estimates, other than the $C_{L\alpha}$ estimate, exhibited erratic behavior. Sensitivity to measurement noise and inaccuracies was the apparent cause of the behavior. This behavior was also observed in results obtained by applying the H^∞ PID algorithm to simulated flight dynamics measurements.

The H^∞ algorithm was tuned so that the final S/C derivative estimates were relatively insensitive to the value of the initial estimate, and hence was predominantly affected by the excitation of the elevator doublet in the data window. The same tuning values were used for all simulation cases. This insensitivity to initial conditions is illustrated in Figs. 23-26, which display the $C_{L\alpha}$, $C_{M\alpha}$, C_{Mq}, and $C_{M\delta e}$ estimates, respectively, for seven different simulations, each using the same clear-air flight test data but a different initial condition. In these figures, the variations in the final values are shown to be a small fraction of the variations in the initial values. The difficulty with the drag derivative estimates and the lift derivative estimates, other than $C_{L\alpha}$, was manifested in the inability to tune the algorithm so that these estimates converged near a single value for different initial conditions. When the algorithm gain was small, these estimates did not react sufficiently to the doublet input to converge and, as the gain was increased, the estimates exhibited too much sensitivity to turbulence and/or measurement noise to converge. Interestingly, while convergence was obtained for $C_{L\alpha}$ estimates in higher velocity cases, in cases with lower velocity, convergence could not be obtained for $C_{L\alpha}$ estimates. On the other hand, convergence was obtained for the pitching moment derivatives in these lower velocity cases. Having established, for the most part, the relative insensitivity of the algorithm to its initial derivative estimates for $C_{L\alpha}$, $C_{M\alpha}$, C_{Mq}, and $C_{M\delta e}$, subsequent simulations used the SIDPAC estimates as initial conditions. Figs. 27–30 depict the $C_{L\alpha}$, $C_{M\alpha}$, C_{Mq}, and $C_{M\delta e}$ estimates, respectively, for a natural icing case without turbulence. In each figure, the straight gray line represents the SIDPAC estimate.

The validation for both lower velocity and higher velocity sections of flight tests is given in Tables 2-5. Results for lower velocity cases are not listed in Table 2 because convergence could not be obtained for $C_{L\alpha}$ in those cases. These results showed that the H^{∞} PID pitching derivative estimates and the corresponding SIDPAC estimates agreed to within 21% for all cases considered. Moreover, the SIDPAC and H^{∞} PID estimates for $C_{M\alpha}$ and C_{Mq} agreed to within 13.3%. In the high velocity cases, the H^{∞} PID $C_{L\alpha}$ estimate agreed with the corresponding SIDPAC estimate to within 13.2%. This difference between the estimates of the two ID methods is consistent with discrepancies observed between stability and control derivative estimates of different tests or methods in other contexts,[9,14] Moreover, there appears to be substantial systematic components to the differences. Such biases, to the extent that they are consistent between clear-air and icing cases, would be less of a concern than random differences. This is because ultimately the icing characterization will compare H^{∞} generated derivative estimates for clean and iced cases in network training, and any systematic errors would merely "subtract out".

CONCLUSION

Identification and characterization of the effects of icing on aircraft performance and control is possible through the use of both trim estimation and parameter identification. Stability and control derivatives, particularly $C_{L\alpha}$ and $C_{M\alpha}$, show potential to be indicators of the effect of the icing. For example, changes in $C_{L\alpha}$ of up to 30% were observed in icing conditions. However, the accuracy of the parameter identification was shown to be a strong function of the scaling factors and biases calculated during the data compatibility analysis. Turbulence was found to be the cause of the variations in the biases and scaling factors. It was also shown that parasite drag, a variable that is easily and accurately calculable, is an excellent indicator of the severity of the ice accretion. This was evident in the better than 80% correlation of the parasite drag with the icing severity parameter that was observed. Using both stability and control parameters and trim it is also possible to detect and evaluate the operation of the ice protection system. Finally, using trim values it is also possible to identify the severity, effect and onset of icing. Further investigation of the effects of turbulence and how to negate them will certainly result in a broader range of parameters for accurately characterizing the effects of icing on control.

This technique of identifying icing and deicing, when used with real time algorithms, shows excellent promise for use in the SIS system.

In summary, the following conclusions are made:

- $C_{L\alpha}$ and $C_{M\alpha}$ indicate the effects of icing on the aircraft, but are significantly affected by atmospheric turbulence.
- Parasite drag is an excellent indicator of the severity of the ice accretion, as seen through its correlation with an icing severity parameter, η.
- The effect of IPS operation is visible in both the stability parameters and the parasite drag including: selective deicing, standard deicing boot cycles and full deicing.
- Trim values, especially α, δe and C_D, are excellent indicators of icing severity, onset and its effect on control and performance.
- Using trim values to characterize the effect of icing shows the most promise in terms of accuracy and reliability.
- Further investigation into the effects of atmospheric turbulence is required to improve parameter identification.
- Real-time H^{∞} PID provides pitching moment derivative estimates that are consistent with SIDPAC estimates
- Real-time H^{∞} PID must incorporate translational accelerations in order to provide useful lift derivative estimates.
- Real-time H^{∞} PID provides lift and pitching moment derivative estimates that are consistent with SIDPAC estimates.

ACKNOWLEDGEMENTS

The authors would like to recognize several people who made this research program possible. First, we would like to thank Tom Ratvasky and the pilots and staff at NASA Glenn for their outstanding work with the Twin Otter. A special thanks goes to Dr. Eugene Morelli for providing us with the SIDPAC software as well as technical support. We would also like to thank Dr. Andy Broeren for formulating the flight test plan. Finally, we would like acknowledge the UIUC SIS research group for their support and assistance throughout this project. This research was funded by NASA Grant NAG 3-21235.

REFERENCES

[1] Kanter, M., "Flight Performance on XB-25E Aircraft No. 42-32281 in Natural Ice During February, March and April 1945," AAF Technical Report 5403, 1945.

[2] Ranaudo, R.J., Mikkelsen, K.L., McKnight, R.C., and Perkins, P.J., "Performance Degradation of a Typical Twin Engine Commuter Type Aircraft in Measured

Natural Icing Conditions," AIAA Paper No. 84-0179, 1984.

[3] Ranaudo, R.J., Mikkelsen, K.L., McKnight, R.C., Ide, R.F., Reehorst, A.L., Jordan, J.L., Schinstock, W.C. and Platz, S.J., "The Measurement of Aircraft Performance and Stability and Control after Flight through Natural Icing Conditions," AIAA Paper No. 86-9758, 1986.

[4] Ratvasky, T.P. and Ranaudo, R.J., "Icing Effects on Aircraft Stability and Control Determined from Flight Data," AIAA Paper No. 93-0398, 1993.

[5] Ratvasky, T.P., Van Zante, J.F., Sim, A., "NASA/FAA Tailplane Icing Program: Flight Test Report," NASA/TP 2000-209908, 2000.

[6] Bragg, M.B., Selig, M.S., Perkins, W.R., Sarter N.B., Basar, T., Voulgaris, P.G. and Melody, J.W., "Smart Icing Systems for Aircraft Icing Safety," AIAA Paper No. 2002-0813, Reno, NV, 2002.

[7] Bragg, M.B., Hutchison, T, Merret, J., Oltman, R., and Pokhariyal, D., "Effect of Ice Accretion on Aircraft Flight Dynamics," AIAA Paper No. 2000-0360, Reno, NV, January 10-13, 2000.

[8] Pokhariyal, D., Bragg, M.B., Hutchison, T, and Merret, J., "Aircraft Flight Dynamics with Simulated Ice Accretion," AIAA Paper No. 2001-0541, Reno, NV, January 8-11, 2001.

[9] Whalen, E., Lee, S., Bragg, M.B., and Ratvasky, T.P., "Characterizing the Effect of Icing on Aircraft Performance and Control from Flight Data," AIAA Paper No. 2002-0816, Reno, NV, January, 2002.

[10] Morelli, E.A., "System Identification Programs for AirCraft (SIDPAC) - Version 1.0 Release Notes," NASA Langley Research Center, Hampton, VA., Jan. 22, 2001.

[11] Melody, J.W., Basar, T., Perkins, W.R., and Voulgaris, P.G., "Parameter Identification for Inflight Detection and Characterization of Aircraft Icing," *Controls Engineering Practice: A Journal of the IFAC*, v.8 n.9, September, 2000.

[12] Melody, J.W., Hillbrand, T., Basar, T., and Perkins, W.R., "H^{∞} Parameter Identification for Inflight Detection of Aircraft Icing: The Time-varying Case," accepted for publication in *Controls Engineering Practice: A Journal of the IFAC*.

[13] Bragg, M.B., T. Hutchinson, J. Merret, R. Oltman and D. Pokhariyal, "Effects of Ice Accretion on Aircraft Flight," AIAA Paper No. 2000-0360, Reno, NV, January 2000.

[14] Batterson, J.G., and O'Mara, T., "Estimation of Longitudinal Stability and Control Derivatives for an Icing Research Airplane from Flight Data," NASA TM-4099, March 1989.

Table 1: Test matrix of phase I of the SIS flight test.

Case	Icing Flight	Doublet Mag.	Test Information
1.1	Clear Air	0.25g	Baseline
1.2	Clear Air	0.10 to 0.50	Vary doublet magnitude
1.3	Clear Air	None	Standard maneuvers
1.4	Clear Air	None	Clear air turbulence
2.1	Icing	0.25g	Doublets during ice accretion
2.2	Icing	0.25g	Doublets with selective deicing
2.3	Icing	0.25g	Doublets with intercycle icing
2.4	Icing	None	Intercycle icing
2.5	Icing	None	Standard maneuvers

Table 2 H^{∞} $C_{L\alpha}$ Validation with SIDPAC Results

		SIDPAC Values	H^{∞} Values	% Difference
Clear Air	High Velocity (9)			
	Mean	0.1081	0.1185	9.70%
	Range	[0.1067,0.1096]	[0.1172,0.1196]	[8.0,11.5]%
	Low Velocity (17)	N/A	N/A	N/A
Natural Icing	High Velocity (3)			
	Mean	0.1092	0.1201	10.00%
	Range	[0.1080,0.1103]	[0.1158,0.1248]	[7.2,13.2]%
	Low Velocity (5)	N/A	N/A	N/A

Table 3 H^{∞} $C_{M\alpha}$ Validation with SIDPAC Results

		SIDPAC Values	H^{∞} Values	% Difference
Clear Air	High Velocity (9)			
	Mean	-0.0269	-0.0284	5.40%
	Range	[-0.0274,-0.0262]	[-0.0287,-0.0279]	[4.2,6.7]%
	Low Velocity (17)			
	Mean	-0.0268	-0.0292	9.00%
	Range	[-0.0287,-0.0255]	[-0.0322,-0.0270]	[5.1,12.5]%
Natural Icing	High Velocity (3)			
	Mean	-0.0295	-0.0309	4.80%
	Range	[-0.0300,-0.0287]	[-0.0324,-0.0294]	[-0.9,8.0]%
	Low Velocity (5)			
	Mean	-0.0295	-0.0317	7.40%
	Range	[-0.0306,-0.0280]	[-0.0329,-0.0300]	[5.1,8.9]%

Table 4 H^{∞} $C_{M\delta e}$ Validation with SIDPAC Results

		SIDPAC Values	H^{∞} Values	% Difference
Clear Air	High Velocity (9)			
	Mean	-0.0314	-0.0346	10.50%
	Range	[-0.0321,-0.0306]	[-0.0351,-0.0341]	[7.5,13.3]%
	Low Velocity (17)			
	Mean	-0.0334	-0.0351	5.20%
	Range	[-0.0346,-0.0313]	[-0.0357,-0.0343]	[2.3,10.1]%
Natural Icing	High Velocity (3)			
	Mean	-0.0314	-0.0328	4.50%
	Range	[-0.0323,-0.0299]	[-0.0343,-0.0300]	[0.3,7.7]%
	Low Velocity (5)			
	Mean	-0.0309	-0.0333	7.70%
	Range	[-0.0321,-0.0296]	[-0.0351,-0.0316]	[4.5,10.3]%

Table 5 H^{∞} C_{Mq} Validation with SIDPAC Results

		SIDPAC Values	H^{∞} Values	% Difference
Clear Air	High Velocity (9)			
	Mean	-35.365	-41.43	17.20%
	Range	[-36.411,-33.662]	[-42.193,-40.269]	[13.4,20.9]%
	Low Velocity (17)			
	Mean	-36.355	-39.372	8.30%
	Range	[-39.711,-34.834]	[-42.247,-37.627]	[4.0,16.8]%
Natural Icing	High Velocity (3)			
	Mean	-35.459	-38.815	9.30%
	Range	[-37.745,-32.415]	[-42.475,-34.244]	[5.6,12.5]%
	Low Velocity (5)			
	Mean	-34.61	-39.077	12.90%
	Range	[-36.165,-32.933]	[-41.833,-36.869]	[8.0,17.2]%

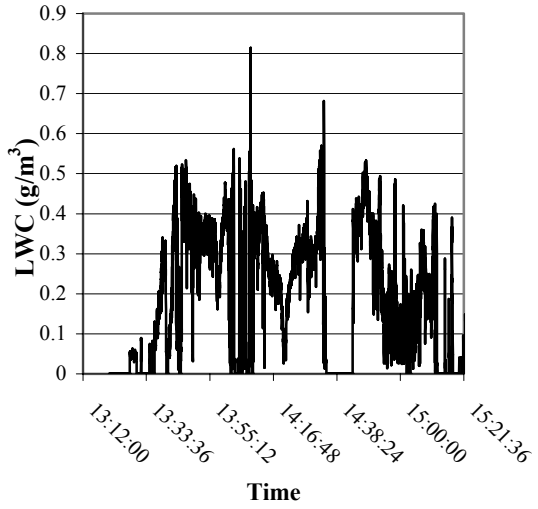

Fig. 1 LWC for Flight 010302f1

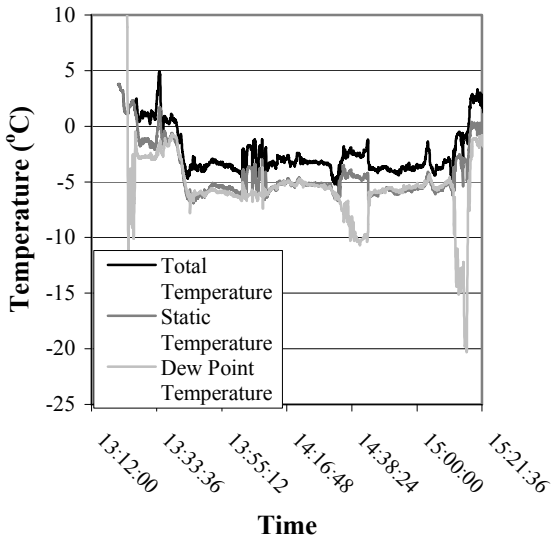

Fig. 2 Temperatures for Flight 010302f1

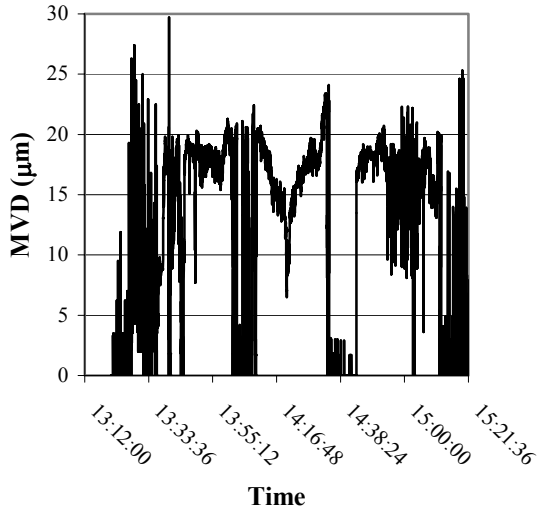

Fig. 3 MVD for Flight 010302f1

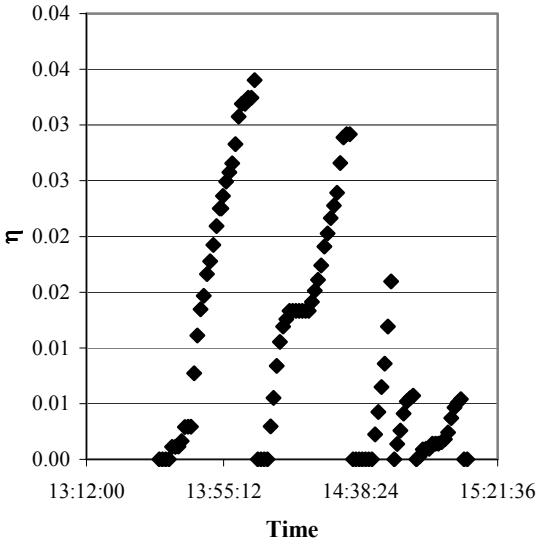

Fig. 4 η for Flight 010302f1

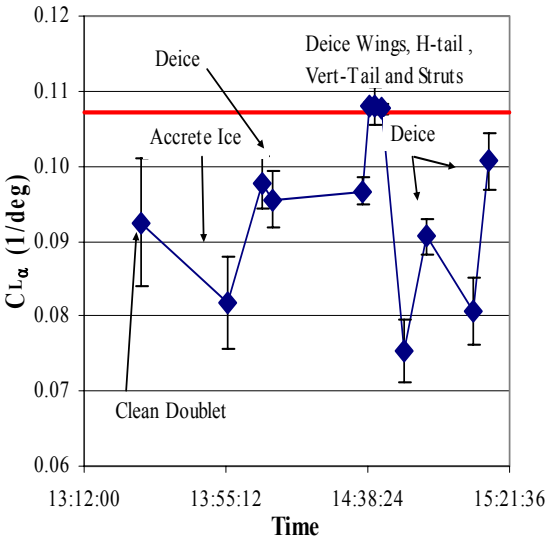

Fig. 5 $C_{L\alpha}$ for Flight 010302f1

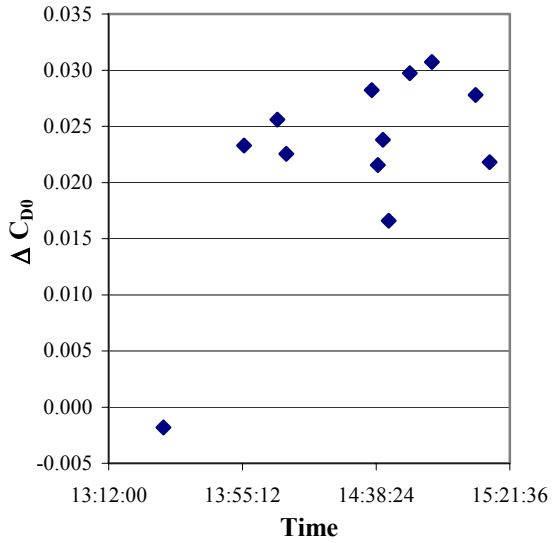

Fig. 7 ΔC_{D0} for Flight 010302f1

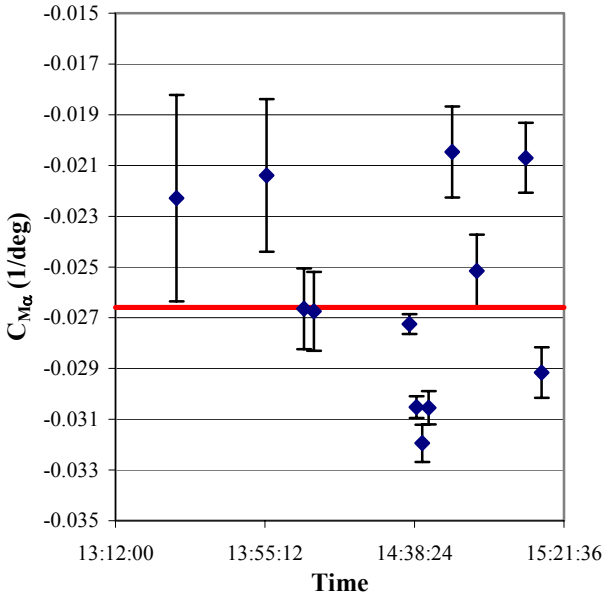

Fig. 6 $C_{M\alpha}$ for Flight 010302f1

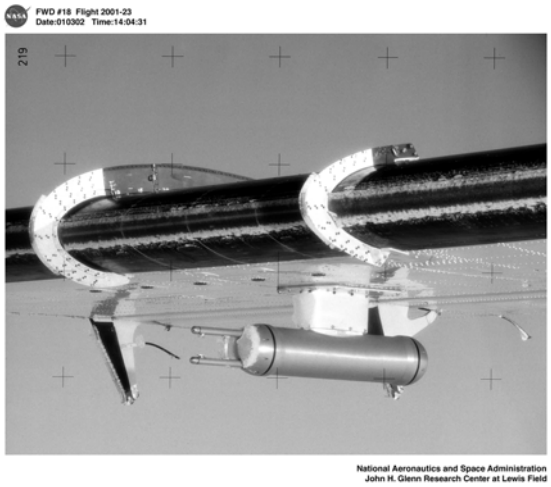

Fig. 8 Wing Leading Edge at 14:04:31

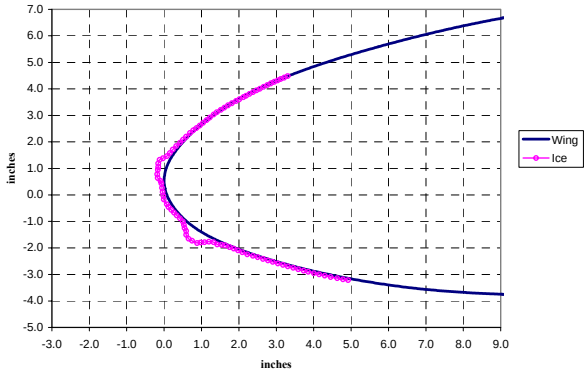

Fig. 9 Ice Profile at 14:04:31

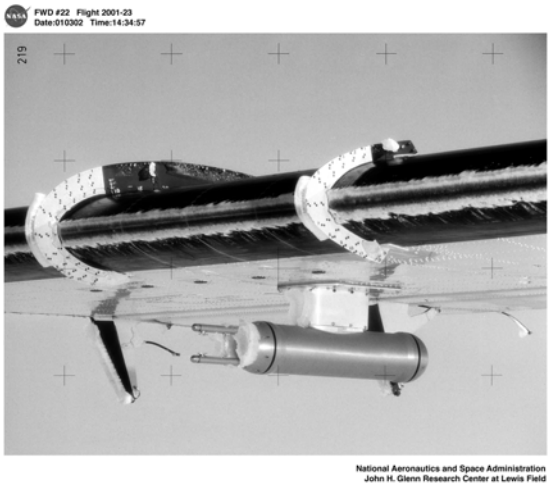

Fig. 10 Right Wing Leading Edge at 14:34:57

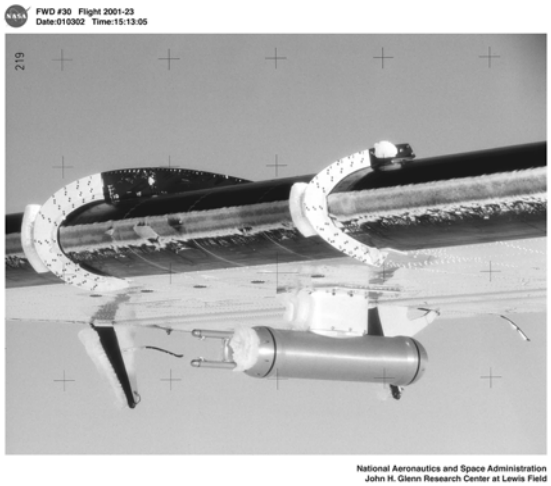

Fig. 13 Right Wing Leading Edge at 15:13:05

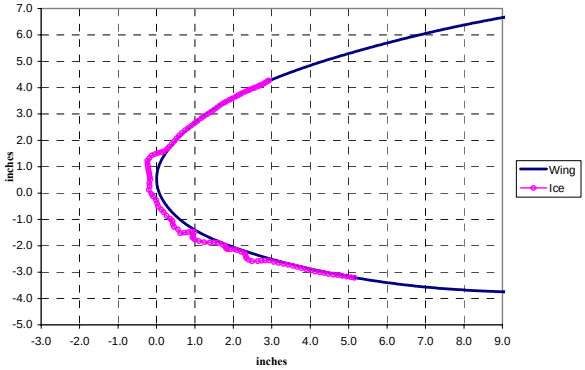

Fig. 11 Ice Profile at 14:34:57

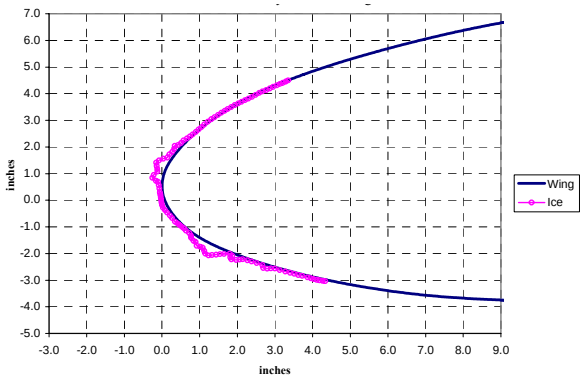

Fig. 14 Ice Profile at 15:13:05

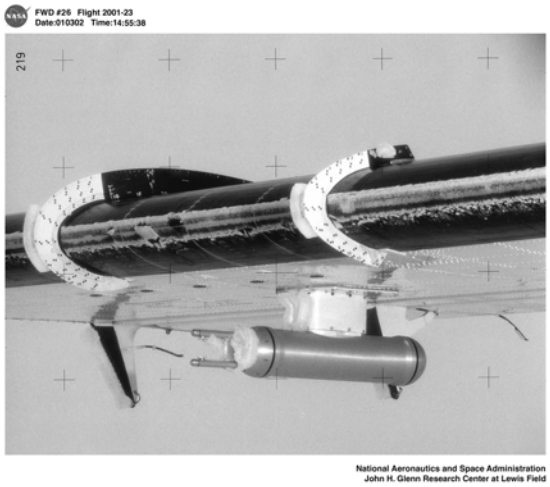

Fig. 12 Right Wing Leading Edge at 14:55:38

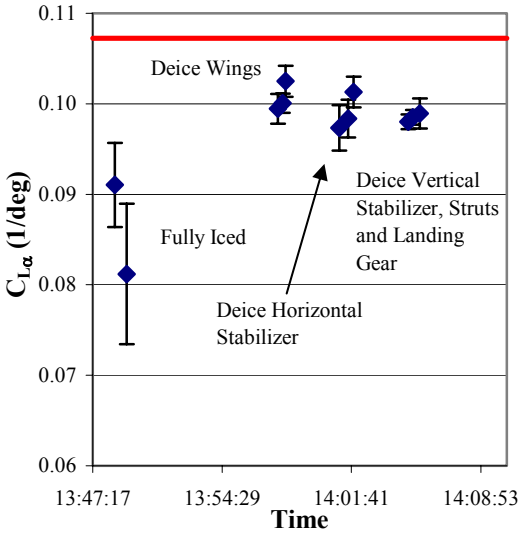

Fig. 15 $C_{L\alpha}$ During Selective Deicing

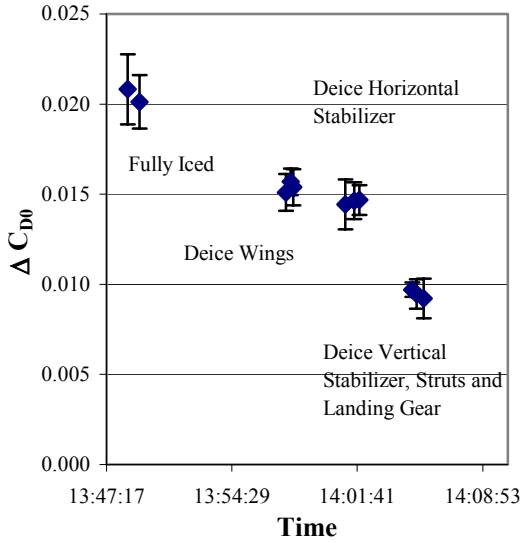

Fig. 16 ΔC_{D0} During Selective Deicing

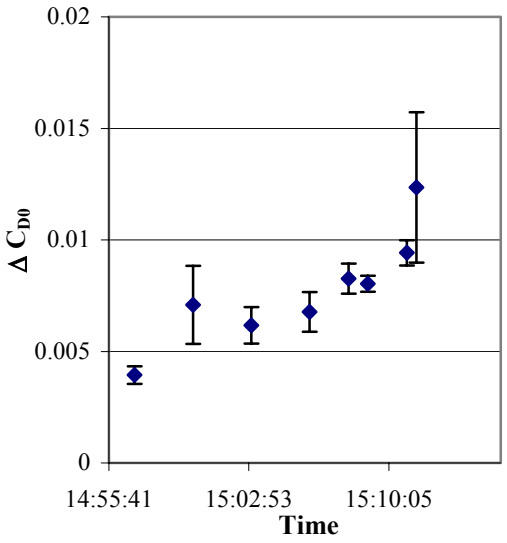

Fig. 18 ΔC_{D0} with the Deicing Boots on a Three Minute Cycle

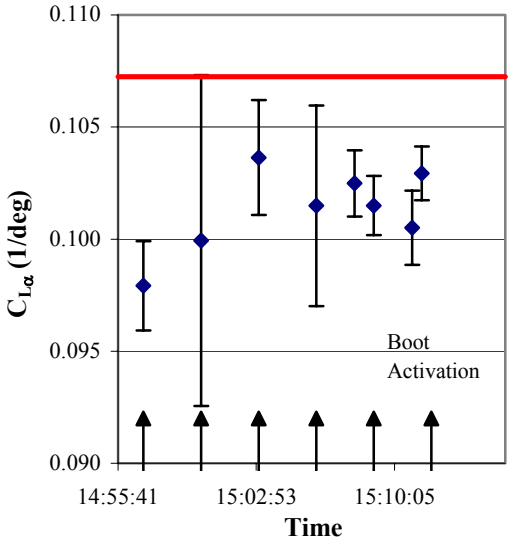

Fig. 17 $C_{L\alpha}$ with the Deicing Boots on a Three Minute Cycle

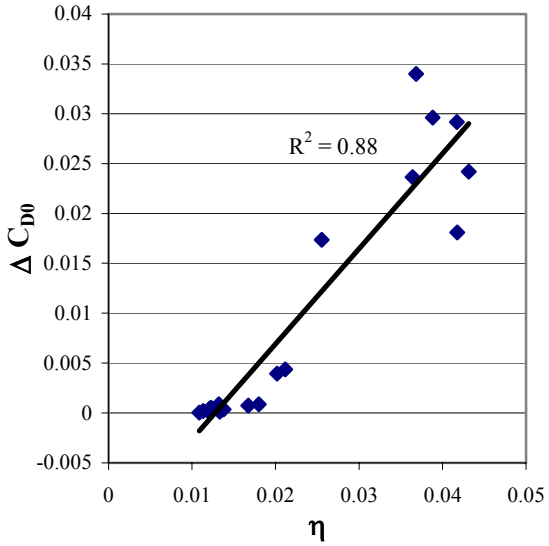

Fig. 19 ΔC_{D0} versus η

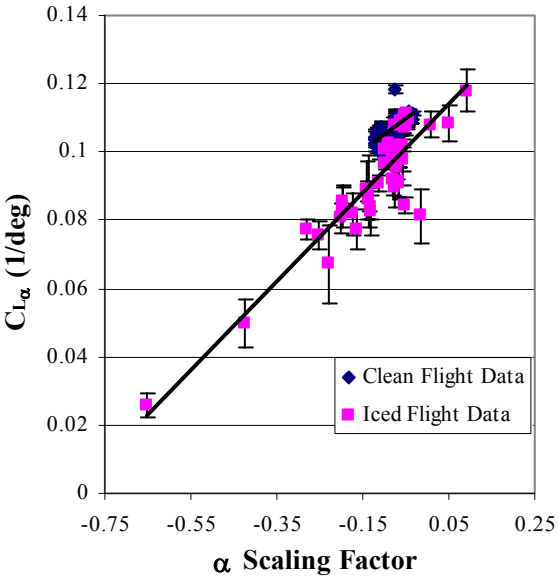

Fig. 20 Variation of $C_{L\alpha}$ with the α Scaling Factor

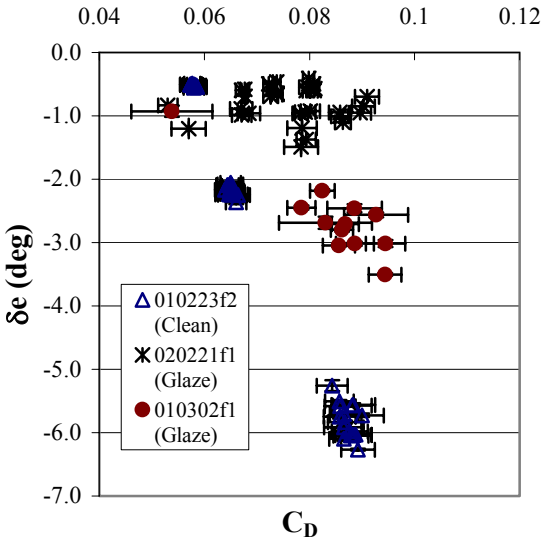

Fig. 21 Elevator Deflection versus Drag Coefficient for Various Flights

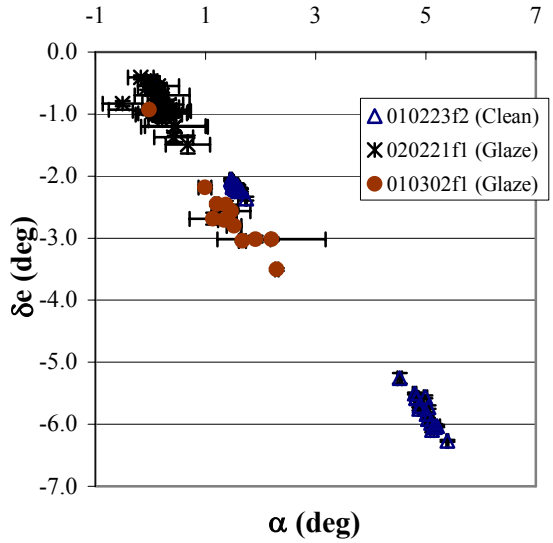

Fig. 22 Elevator Deflection versus Angle of Attack for Various Flights

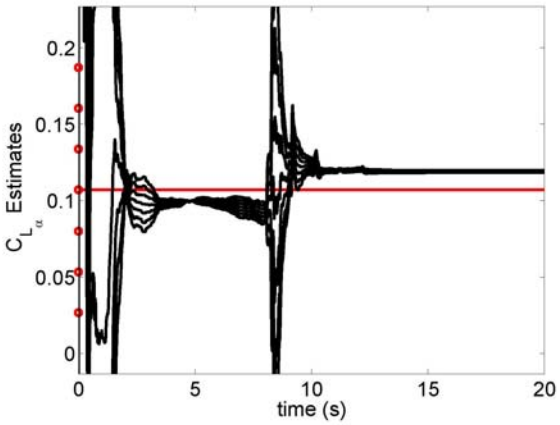

Fig. 23 H^{∞} ID Estimates of $C_{L\alpha}$ in Clear Air for Various Initial Conditions with Corresponding SIDPAC Estimate (gray)

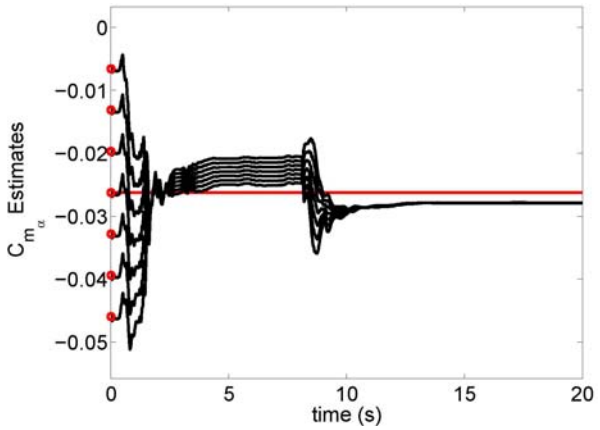

Fig. 24 H^{∞} ID Estimates of $C_{M\alpha}$ in Clear Air for Various Initial Conditions with Corresponding SIDPAC estimate (gray)

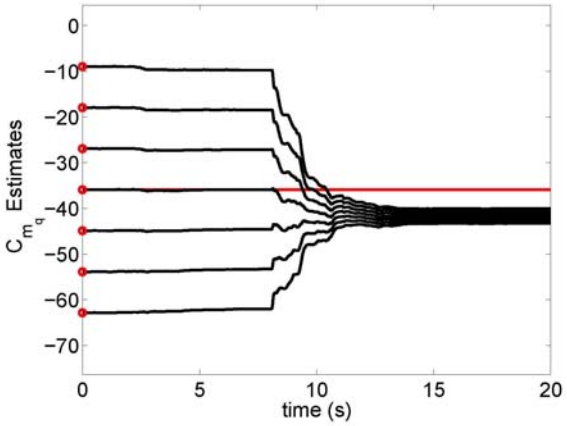

Fig. 25 H^{∞} ID Estimates of C_{Mq} in Clear Air for Various Initial Conditions with Corresponding SIDPAC Estimate (gray)

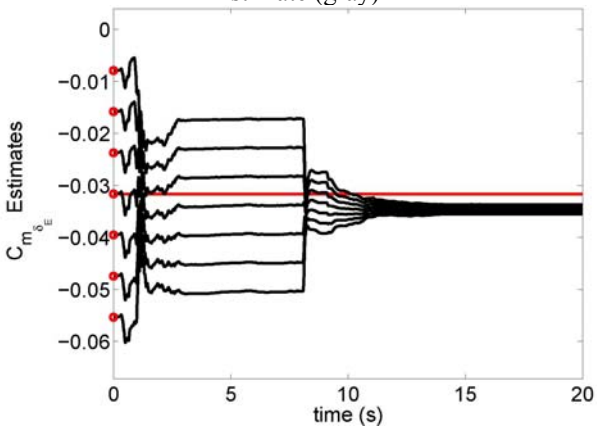

Fig. 26 H^{∞} ID Estimates of $C_{M\delta e}$ in Clear Air for Various Initial Conditions with Corresponding SIDPAC estimate (gray)

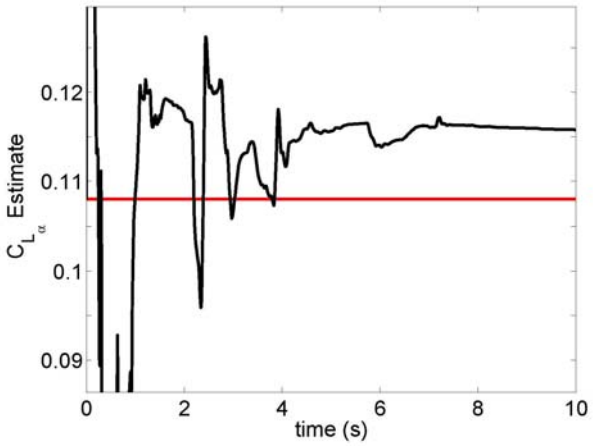

Fig. 27 H^{∞} ID Estimate of $C_{L\alpha}$ in Natural Icing with Corresponding SIDPAC Estimate (gray)

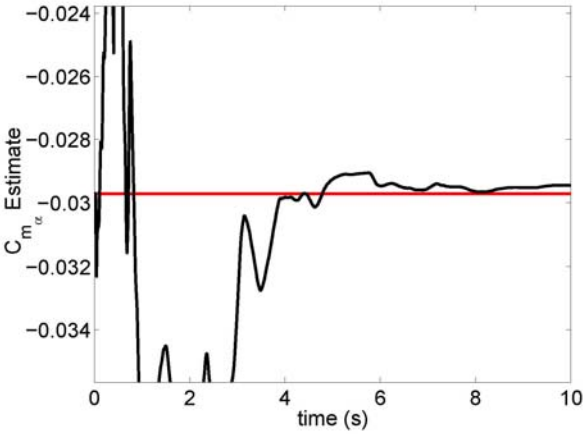

Fig. 28 H^{∞} ID Estimate of $C_{M\alpha}$ in Natural Icing with Corresponding SIDPAC Estimate (gray)

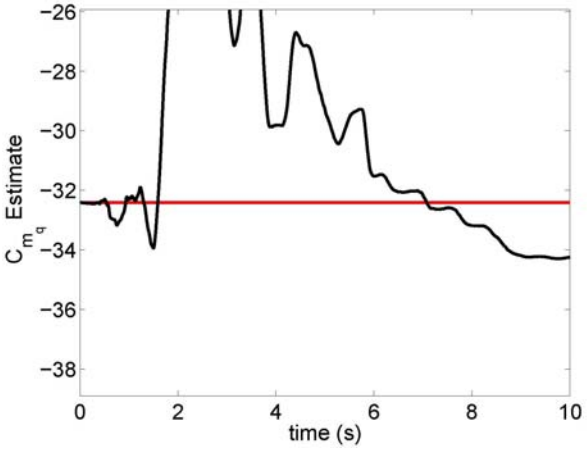

Fig. 29 H^{∞} ID Estimate of C_{Mq} in Natural Icing with Corresponding SIDPAC Estimate (gray)

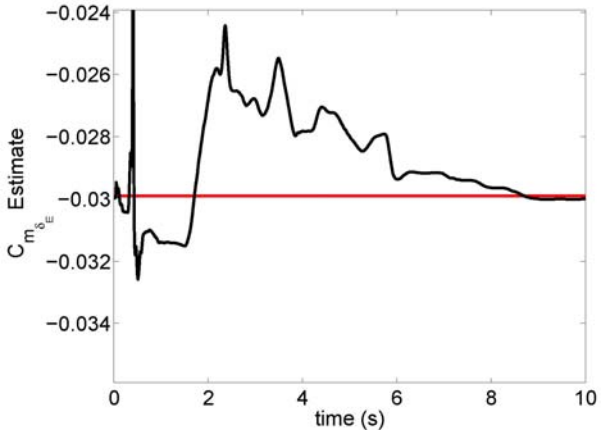

Fig. 30 H^{∞} ID Estimate of $C_{M\delta e}$ in Natural Icing with Corresponding SIDPAC Estimate (gray)